ACS OMEGA

Open Access

http://pubs.acs.org/journal/acsodf

Article

Multiband $MgAl_{0.05}Ge_{0.95}O_3$:0.3%Pr^{3+} Persistent Phosphor as Efficient Tracers in Crude Oil Emulsions

Syed Niaz Ali Shah* and Yafei Chen

Cite This: *ACS Omega* 2024, 9, 38678−38685

Read Online

ACCESS | Metrics & More | Article Recommendations | Supporting Information

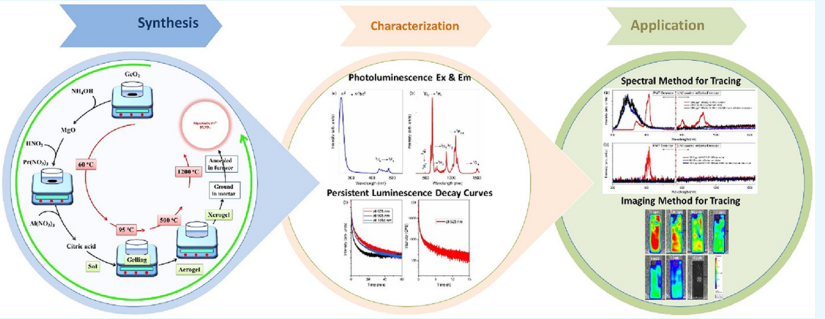

ABSTRACT: The use of fluorescent nanoparticles (NPs) for tracing purposes in oilfields encounters challenges due to background interferences under constant external excitation caused by organic residues present in crude oil. This results in insufficient sensitivity and lower tracer detection limits in the crude oil/water emulsions. In this study, we present the synthesis of persistent luminescent NPs, showcasing their remarkable application as tracers in crude oil. The multiband $MgAl_{0.05}Ge_{0.95}O_3$:0.3%Pr^{3+} persistent NPs were synthesized via the sol−gel method. Through meticulous experimentation and analysis, our study unveils a novel avenue for efficient and lasting traceability in crude oil. The synthesized NPs emit light across the visible, near-infrared, and shortwave infrared regions, allowing for versatile detection. The unique luminescent properties of these NPs, particularly their ability to persist in emitting light without a continuous external excitation, enable their effective use as tracers in crude oil/water emulsions where background fluorescence typically poses a significant challenge. By employing these persistent NPs in background fluorescence-free conditions, we achieve ultrahigh sensitivity in detecting these NPs in crude oil. Our research reveals that the doping of Al^{3+} ions significantly enhances both the afterglow intensity of $MgGeO_3$:0.3%Pr^{3+} phosphor and the afterglow decay time of Pr^{3+} emission. This characteristic enables the re-excitation of $MgAl_{0.05}G_{0.95}O$:0.3%Pr^{3+} NPs within the emulsion, allowing for repeated spectral and imaging acquisition. This high sensitivity not only facilitates precise imaging of NPs in crude oil but also enables long-term monitoring in real-time, offering valuable insights for oilfield operations.

1. INTRODUCTION

In the dynamic landscape of the oil industry, the need for effective tracing methods is crucial for monitoring the movement and distribution of crude oil. In this context, the synthesis and utilization of persistent luminescent nanoparticles (NPs) represent a groundbreaking advancement, offering a promising solution for enhancing the efficiency and accuracy of crude oil tracing. This is due to its unique properties, such as high stability, distinct signal detection capabilities, and minimal interference with the crude oil matrix. These characteristics make it an ideal tracer, ensuring the precise and reliable monitoring of crude oil movements. Persistent luminescence, a fascinating phenomenon wherein materials continue to emit light for minutes to hours after the excitation source is removed, has garnered significant attention in recent years.[1−3] Visible persistent phosphors, widely employed across various domains, have garnered significant commercial success.[4,5] However, the recent surge of interest has shifted toward the near-infrared (NIR, 700−900 nm)[6] and the short-wave infrared (SWIR, 900−1700 nm),[7,8] particularly in applications such as biomedical imaging and night-vision surveillance. The standout feature of persistent luminescence materials is their ability to self-illuminate, which enables excitation-free imaging in an autofluorescence-free manner, thus ensuring a high signal-to-noise ratio and high sensitivity,[9] in contrast to the photoluminescent[10] and other luminescent methods.[11,12] There is an interest in the Pr^{3+} emission due to its potential applications in display technology, lighting, security, and healthcare.[13] The versatility of Pr^{3+} lies in its

Received: May 11, 2024
Revised: July 23, 2024
Accepted: August 19, 2024
Published: September 4, 2024

various intraconfigurational transitions of $4f^2$ states and other interconfigurational $4f^15d^1$ states, resulting in luminescence across ultraviolet (UV), visible, NIR, and shortwave infrared (SWIR) regions when incorporated in different host materials, making it favorable for getting different colors and potential applications. For instance, the red emission from the $^1D_2$ state of the Pr^{3+} has found utility in vacuum fluorescent and field emission displays.[14]

In the realm of enhanced oil recovery, accurate and reliable tracing methods are of paramount importance to monitor the flow and distribution of crude oil.[15] Persistent luminescent NPs have emerged as a promising solution, offering distinct advantages over conventional tracing techniques.[16] These NPs can be selectively doped and functionalized to exhibit tunable emission properties and dispersibility in both water and oil, enabling their effective deployment as tracers in complex crude oil systems. Recent studies have demonstrated successful applications of upconversion NPs as tracers for production and well monitoring.[16] The flow experiments using stable crude oil emulsion have shown that these NPs tracers can effectively flow through porous media and be distinguished from one another, even in the presence of organic components. This capability can often open new avenues for in situ reservoir communication and understanding, allowing for more efficient monitoring and management of crude oil resources. The reservoir characterization is necessary and often facilitated by specially designed reservoir tracers. Typically, chemical and radioactive tracers have been utilized and proven useful, although environmental concerns and costly analytical techniques limit the use of these tracers. Nanotechnology holds promise in addressing these limitations.[17,18] Recently, carbon dots and rare-earth-doped NPs have been used as tracers. Despite their advantages, these tracers suffer from lower sensitivity in crude oil, mainly due to autofluorescence from crude oil under constant external excitation. To suppress the autofluorescence interferences from the oil samples, necessitating the use of long-lifetime fluorescence nanomaterials. However, their poor detection limit also limits their use for practical applications. Thus, it is necessary to develop and use new tracers that are nonradioactive and are stable in harsh reservoir environments and can be used in standard laboratories. To overcome these challenges, the use of persistent luminescence NPs presents a compelling solution. These materials capture and gradually release stored energy from electrons to the emitting center in the materials, resulting in prolonged emission even after the excitation source is removed.[19] Furthermore, the convenient analysis of these NPs using relatively simple or portable instruments presents a significant advantage over traditional tracers that often require complex and expensive analytical techniques.[16,20,21] Recently, $CaTiO_3:Pr^{3+}$ persistent luminescent NPs were used as tracers in the crude oil/water emulsion.[22] Moreover, $LiGa_5O_8:Cr^{3+}$ persistent luminescence NPs, which emit NIR emission at 716 nm after excitation in the UV region, were used for highly sensitive detection in a crude oil−water emulsion.[23] The exceptional detection limit (1 ppb) of this imaging method underscores the utility of multiband persistent luminescence nanomaterials capable of emitting across visible, NIR, and SWIR regions.

Synthesis methodologies significantly influence the properties of the persistent luminescence materials. The persistent luminescence materials are synthesized using different methodologies[19,24] but are mostly synthesized by the solid-state method which results in large particle sizes and passive surfaces. For instance, Liang et al. synthesized $MgGeO_3:Pr^{3+}$ phosphor via a solid-state high-temperature technique,[25] encountering challenges such as compositional inhomogeneity, high processing temperature, and nonuniform particle sizes. In this context, we used the citrate sol−gel method to prepare $MgAl_{0.05}Ge_{0.95}O_3:0.3\%Pr^{3+}$ NPs. The prepared $MgAl_{0.05}G_{0.95}O_3:0.3\%Pr^{3+}$ NPs exhibit emission peaks at 625 nm (visible), 905 nm (NIR), and 1089 nm (SWIR). The resulting materials not only offer emission across different wavelengths but also boast long persistent luminescence, presenting significant advantages for spectral and imaging applications in the oil field without the need for an in situ excitation source, with potential future applications in bioimaging.

2. EXPERIMENTAL SECTION

2.1. Chemicals. GeO_2 (99.999% purity) was purchased from GFI, Advanced Technologies, Inc., USA. $Al(NO_3)_3\cdot 9H_2O$ (with a purity range of 98.0−102%), NH_4OH (with 28% NH_3 concentration), MgO (99.99% purity), and $Pr(NO_3)_3\cdot 6H_2O$ (99.99% purity) were purchased from Alfa Aesar, ThermoFisher (Kandel) GmbH, Germany. HNO_3 (69% concentration) was purchased from Loba Chemie Pvt. Ltd., Mumbai, India. Citric acid (≥99.5%) was obtained from Honeywell International India Pvt. Ltd., India. All solutions were prepared using deionized water.

2.2. Synthesis and Characterization of $MgAl_{0.05}Ge_{0.95}O_3:0.3\%Pr^{3+}$ Nanophosphor. The $MgAl_{0.05}Ge_{0.95}O_3.0.3\%Pr^{3+}$ phosphor was synthesized using the citrate sol−gel method with subsequent calcination. Initially, the corresponding nitrates of the metals were dissolved in DI water, and citric acid was used as a complexing agent. The stoichiometric amount of GeO_2 was added to 20 mL of DI water, followed by the addition of NH_4OH and MgO. The MgO was then converted to its nitrate form by the addition of HNO_3. $Pr(NO_3)_3$ was added to the above mixture, followed by the addition of $Al(NO_3)_3$. Lastly, citric acid was added to the reaction mixture, maintaining a molar ratio of metal cations to citric acid at 1:2. The solution was stirred and heated at 60 °C and then dehydrated at 95 °C to form the polymeric complex. After overnight incubation at 95 °C to form a foam with enormous swelling, the sample was then combusted on a hot plate at 500 °C to yield a fine black powder. The powder was ground using a mortar and then transferred to ceramic crucibles for calcination at various temperatures and durations to achieve the desired phosphor material.

Particle size refinement was achieved through grinding using a MICROCER grinder from NETZSCH Micro & Mini-Serie (2801047-10), Feinmahltecnik GmbH. The $MgAl_{0.05}Ge_{0.95}O_3.0.3\%Pr^{3+}$ particles underwent grinding for 3 h in different solvents, and the large particles were subsequently removed via centrifugation at lower rpm. Finally, the particles were freeze-dried using a Millrock Bench-Top Freeze-Dryer. The size and distribution of the as-synthesized $MgAl_{0.05}Ge_{0.95}O_3:0.3\%Pr^{3+}$ NPs were assessed using a Zetasizer Nano-ZS, Malvern, U.K.

The synthesis of the $MgAl_{0.05}Ge_{0.95}O_3.0.3\%Pr^{3+}$ phosphor involved several steps, including the dissolution of metal nitrates, the addition of complexing agents, and the formation of a polymeric complex through heating and dehydration. The resulting powder was then calcined at various temperatures to

https://doi.org/10.1021/acsomega.4c04281
ACS Omega 2024, 9, 38678−38685

obtain the desired phosphor material with the desired particle distribution.

2.3. Spectral Characterization. The spectral characterizations were conducted using a Horiba NanoLog spectrofluorometer equipped with a 75 W xenon arc lamp, an R928 photomultiplier tube (PMT), and an LN2-cooled InGaAs (DSS-IGA020L) detector. The photoluminescence excitation and emission spectra, persistent luminescence emission spectra, and persistent luminescence decay curves were acquired. The spectra analysis from 300 to 850 nm was done using a PMT detector, while the liquid nitrogen-cooled InGaAs detector was used for measurement from 850 to 1550 nm. For persistent luminescence spectra and decay curves, the samples were excited by using a 254 nm UV lamp. To avoid stray light in the spectral measurements, we used appropriate optical filters.

2.4. Detection of $MgAl_{0.05}G_{0.95}O_3$:0.3%Pr^{3+} NPs in Oil/Water Emulsion. The unrefined crude oil from Saudi Arabia was used without any pretreatment. The different amounts of $MgAl_{0.05}G_{0.95}O_3$:0.3%Pr^{3+} dispersed in water were mixed with the crude oil in a 50/50 volume ratio or otherwise specified to form the emulsions. Measurements were conducted using 3.5 mL quartz cuvettes with a 10 mm path length utilizing a Horiba NanoLog spectrofluorometer for spectral acquisition.

Imaging of the samples was performed using an IVIS Lumina III imaging system (PerkinElmer) equipped with a cooled charge-coupled device (CCD) camera in bioluminescence mode. The samples, containing $MgAl_{0.05}G_{0.95}O_3$:0.3% Pr^{3+} NPs dispersed in water and crude oil within quartz cuvettes, were subjected to irradiation with 254 nm UV light for 5 min. Images were captured at intervals of 15 s, 30 s, and 1 min of the stoppage of excitation. Different exposure times, namely 30 s and 1 min, were tried for image acquisition. The images were processed by living image software (Version 4.7.2, PerkinElmer, Inc.). To ensure comparability, images were captured under similar conditions. The average intensity was found by processing the acquired images by Living Image software at a binning of 8 and smoothing of 3 × 3 by the region of interest (ROI) tool.

3. RESULTS AND DISCUSSION

In the quest for innovative solutions to enhance crude oil tracing, we successfully synthesized persistent luminescent NPs that hold promise for revolutionizing the oil industry. The synthesis of the $MgAl_{0.05}Ge_{0.95}O_3$:0.3%Pr^{3+} nanophosphor was accomplished through the sol−gel method, where the proportions of various reactants and synthesis parameters were carefully tuned to achieve heightened persistent luminescence intensity. The optimization process proved crucial in enhancing the persistent luminescence intensity and the persistent luminescence decay time of the synthesized phosphor, a feat predominantly facilitated by codoping of Al^{3+} ions alongside Pr^{3+}. Notably, an optimal Al^{3+} concentration of 5 mol % was identified to yield the most favorable results.

Characterization through X-ray diffraction measurements revealed the synthesized phosphor to possess an orthorhombic (ilmenite) structure, consistent with the host materials $MgGeO_3$, unaffected by the doping of Pr^{3+} and Al^{3+} (Figure S1), which is discussed in detail previously.[26,27] However, annealing at higher temperatures was found to augment persistent luminescence properties, although the high temperature causes the formation of intrinsic defects resulting in large sizes of the materials.[19] Luminescent materials doped with transition or rare earth ions have shown promise for a wide range of applications, including communication devices, where the luminescent efficiency can be enhanced by adding small amounts of activator ions to the host lattice.[28] The unique optical properties of luminescent NPs, such as those synthesized in this work, can be analyzed by relatively simple or even portable spectral instruments, making them attractive alternatives to traditional tracers.

The undoped $MgGeO_3$:Pr^{3+} sample exhibited poor persistent luminescence, which was greatly improved by the introduction of the Al^{3+} ion as a codopant (Figure S2). The ionic radius of the Al^{3+} ion (0.675 Å) is similar to that of the substituted Ge^{4+} ion (0.67 Å), allowing it to occupy the hexacoordinated Ge^{4+} sites in the $MgGeO_3$ lattice. The incorporation of the trivalent Al^{3+} ions into the tetravalent Ge^{4+} sites creates a charge mismatch, leading to the spontaneous formation of lattice defects for charge compensation.[29] These defects, induced by Al^{3+} doping, serve as potential electron trapping centers, which enhance the persistent luminescence of the $MgAl_{0.05}Ge_{0.95}O_3$:0.3%Pr^{3+} NPs.

The photoluminescence excitation and emission spectra of the synthesized phosphor provided valuable insights into the phosphor's optical properties, as shown in normalized graphs in Figure 1. The excitation spectrum (monitored at 625 nm) in

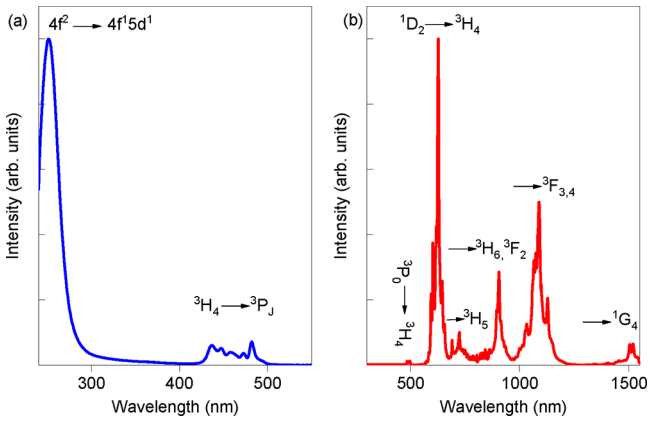

Figure 1. Photoluminescence excitation and emission spectra of the $MgAl_{0.05}Ge_{0.95}O_3$:0.3%Pr^{3+} persistent phosphor. (a) Excitation spectrum was obtained by monitoring at 625 nm emission. (b) Emission spectrum was obtained by 260 nm excitation. The emission from 300 to 850 nm was monitored by a PMT detector, while that from 850 to 1550 nm was monitored by a liquid nitrogen-cooled InGaAs detector.

both the UV region (<300 nm) and blue spectral region (from 430 to 500 nm) elicited distinct responses attributed to various transitions within Pr^{3+} ions and the host materials (Scheme 1). Specifically, the excitation in the UV region (240−300 nm) peaking at 250 nm may be due to the absorption of the host edge[8,9,30] or the interconfigurational transition, $4f^2 \rightarrow 4f^15d^1$.[30,31] The excitation peaks in the blue region (430−500 nm), on the other hand, are associated with the intraconfigurational transition of an electron from the ground state ($^3H_4$) to the ^3P_J excited states of the Pr^{3+} ions.[30]

When the sample was excited at 260 nm, it exhibited emission in the visible, NIR, and SWIR regions. There were three dominant peaks with some small peaks in the emission spectrum. The smaller peak at 430−500 nm was attributed to the $^3P_J \rightarrow ^3H_4$ transition. The emission spectrum of $MgAl_{0.05}Ge_{0.95}O_3$:0.3%Pr^{3+} showcased the dominant peaks

https://doi.org/10.1021/acsomega.4c04281
ACS Omega 2024, 9, 38678−38685

Scheme 1. (a) Schematic of the Energy Levels of Pr^{3+} States in CB and VB of the $MgAl_{0.05}Ge_{0.95}GeO_3$:0.3%$Pr^{3+}$, the $4f^15d^1$ State is in the CB Edge of the Host Material; (b) Diagram Showing the Configuration-Coordinate of the Preferential Feeding of $^1D_2$ State of Pr^{3+} by the Exciton-like State[a]

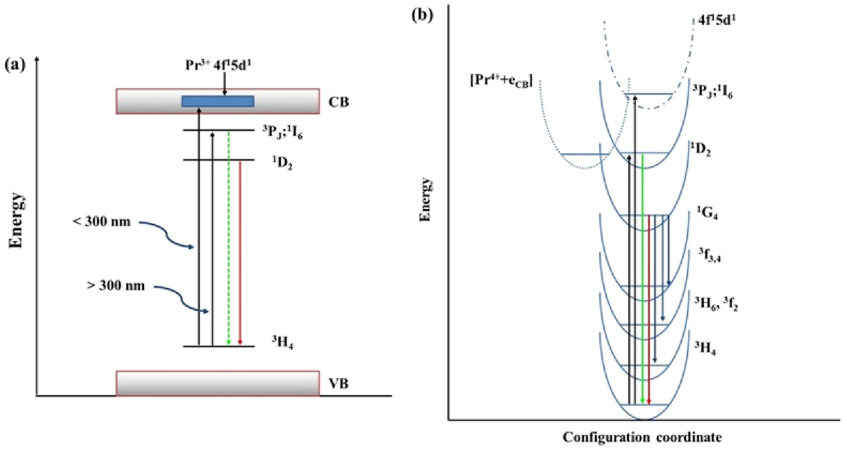

[a]Excitation of the materials happens by the interconfigurational transition, $4f^2 \rightarrow 4f^15d^1$, or via the intraconfigurational transition, $^3H_4 \rightarrow {}^3P_J$. The emission from the $4f^15d^1$ state is quenched by the exciton-like state and funnels the energy to the $^1D_2$ state, which is the dominating emissive state in the $MgAl_{0.05}Ge_{0.95}GeO_3$:0.3%$Pr^{3+}$ materials.

originating from transitions involving the $^1D_2$ state of Pr^{3+} spanning the visible, NIR, and SWIR regions. In the emission spectrum, the emissions were dominated by the transition from the $^1D_2$ state of Pr^{3+} ions. A red emission band peaking at 625 nm in the visible region was attributed to the $^1D_2 \rightarrow {}^3H_4$ transition of the Pr^{3+} ion. The peak at 905 nm in the NIR region was attributed to the $^1D_2 \rightarrow {}^3H_6$, $^3F_2$ transition, and the peak at 1089 nm was attributed to the emission from the $^1D_2 \rightarrow {}^3F_{3,4}$ transition in the SWIR region.[7,25] The peak at 1500 nm was due to the $^1D_2 \rightarrow {}^1G_4$ transition.[7]

The dominance of emission from the $^1D_2$ state and the absence of emission from the ^3P_J state suggest the localization of the $4f^15d^1$ state of Pr^{3+} is in the conduction band of the host material, and the emission involves a trapped exciton-like [$Pr^{4+} + e_{CB}$] state.[13,30,31] The excitation results in an electron from the $^3H_4$ state being promoted to the $4f^15d^1$ state (eq 1) and a subsequent transfer to the conduction band of the host to form an exciton-like state. This exciton-like state bypasses the ^3P_J state and funnels the energy to the $^1D_2$ state (eq 2), which causes the preferential emission from the $^1D_2$ state[31] as explained in Scheme 1. The $4f^15d^1$ state is nonradiatively quenched by the exciton-like state, which results in no emission from $4f^15d^1$ to $4f^2$ as shown in the simplified configuration coordinate scheme.

The presence of metals in the host with nd^0 or nd^{10} (e.g., Ge^{4+}) configurations with metal-to-metal charge transfer transition also accounts for the lack of emission from the ^3P_J state.[32,33] Thus, the dominating emission from the $^1D_2$ state of Pr^{3+} is reasonable. The interplay between the dopant, host materials, and excitation mechanism elucidates the nuanced photoluminescent behavior observed in $MgAl_{0.05}Ge_{0.95}O_3$:0.3% Pr^{3+} nanophosphor, underscoring its potential for various applications in optoelectronics devices.[28]

$$4f^2(^3H_4) \rightarrow 4f^15d^1; {}^3P_{J[=0,1,2]} \quad (1)$$

$$4f^15d^1 \rightarrow {}^1D_2 \quad (2)$$

The dispersion of $MgAl_{0.05}Ge_{0.95}O_3$:0.3%Pr^{3+} in an aqueous medium triggers an intriguing cascade of events. Initially, the $4f^15d^1$ state of Pr^{3+} becomes localized below the conduction band. Subsequently, the excited electron may undergo a transition to a lower energy level, leading to a weak emission from the $^3P_0$ state. The transition from the $4f^15d^1$ state facilitates the feeding of the ^3P_J state in the absence of an exciton-like state, thereby resulting in an observable emission from the ^3P_J state.

Upon exciting the sample with 254 nm UV light for 5 min and then discontinuing the irradiation, the synthesized phosphors exhibited persistent luminescence across the visible, NIR, and SWIR regions (Figure 2).[34,35] Spectra of the persistent luminescence emission were recorded at different decay times ranging from 5 min to 5 h after the excitation of the samples at 254 nm for 5 min (Figure 2a). Notably, the persistent luminescence signal can be easily recorded in the visible, NIR, and SWIR regions after 5 h. Additionally, a comparison of the persistent luminescence emission spectra (Figure S3) with the photoluminescence spectra of the synthesized phosphor confirms that the emission in all the regions is from the same emitting state ($^1D_2$) of the Pr^{3+} ions.

Further analysis involved recording persistent luminescence decay curves at different wavelengths, i.e., 625, 905, and 1089 nm over a period of 1 h (Figure 2b). Remarkably, the persistent luminescence decay curve of the spin-forbidden $^1D_2 \rightarrow {}^3H_4$ transition at 625 nm can be monitored for over 15 h after the stoppage of the excitation (Figure 2c). Mechanistically, excitation in the UV region caused photogenerated electrons, which are subsequently captured and stored by traps in the host material. Upon the cessation of excitation, thermal stimulation causes these stored electrons to return to the excited state of the Pr^{3+} ions, resulting in persistent luminescence across the visible, NIR, and SWIR regions.[35] The ability of these phosphors to emit in the NIR and SWIR regions is particularly promising for bioimaging and night vision applications.

The synthesized phosphors were further assessed for their ability to detect crude oil/water emulsions by using spectral and imaging methods, as discussed in the subsequent sections.

https://doi.org/10.1021/acsomega.4c04281
ACS Omega 2024, 9, 38678−38685

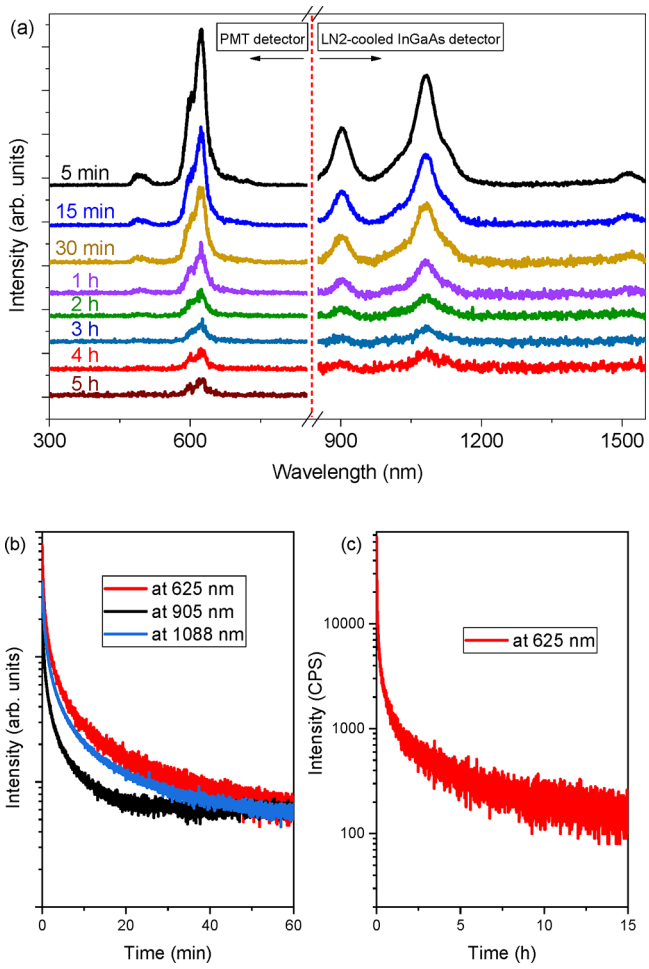

Figure 2. Persistent luminescence emission of the synthesized phosphor. (a) Persistent luminescence emission spectra of the $MgAl_{0.05}Ge_{0.95}O_3$:0.3%Pr^{3+} persistent phosphor were recorded at different decay times from 5 min to 5 h. The spectra from 300 to 850 nm were recorded using a PMT detector, while from 850 to 1550 nm, an InGaAs detector was used. (b) Persistent luminescence decay curves of the $MgAl_{0.05}Ge_{0.95}O_3$:0.3%Pr^{3+} persistent phosphor. The decay curves were obtained by monitoring at 625, 905, and 1088 nm for 1 h after irradiation at 254 nm for 5 min. The emission slit width was 25 nm for the InGaAs detector and 14 nm for the PMT detector. (c) Decay curve was obtained by monitoring at 625 nm for 15 h after irradiation at 254 nm for 5 min. The emission slit width was 14 nm.

3.1. Spectral Method of Determination. The application of luminescent NPs as tracers has been investigated in recent years as an alternative to traditional tracers.[16,20] Luminescent NPs are expected to have similar behavior to molecular tracers, and their unique optical properties can be analyzed by relatively simple or even portable spectral instruments. However, the deployment of these traditional tracers has become more restricted and limited due to either increasing environmental concerns or the need for expensive and inconvenient analytical techniques. The use of persistent luminescence NPs, such as $MgAl_{0.05}Ge_{0.95}O_3$:0.3Pr^{3+} NPs, offers advantages over photoluminescent materials for oil field sensing applications.[20,36]

Initially, the spectral method was tried to detect the presence of $MgAl_{0.05}G_{0.95}O_3$:0.3%Pr^{3+} NPs within the crude oil/water emulsion.[20] These $MgAl_{0.05}G_{0.95}O_3$:0.3%Pr^{3+} NPs, when dispersed in water, exhibited three distinctive bands in their photoluminescence spectra, as depicted in Figure 3a, which is similar to the photoluminescence spectra of the phosphor in the solid-state. Notably, a broad peak ranging from 300 to 600 nm was observed from the oil/water emulsion.[20]

In the case of 50/50 crude oil/water emulsion, only emissions from the oil were detected in the spectra of $MgAl_{0.05}G_{0.95}O_3$:0.3%Pr^{3+} NPs, as illustrated in Figure 3a. However, upon the cessation of excitation, the emission from the oil component disappeared, and the emission from $MgAl_{0.05}G_{0.95}O_3$:0.3%Pr^{3+} NPs became observable, indicating their distinct presence.[16,20]

The persistent luminescence emission from $MgAl_{0.05}G_{0.95}O_3$:0.3%Pr^{3+} NPs within water, oil/water, and 50/50 water/oil emulsions is displayed in Figure 3b. The spectral outcomes underscore the advantages of persistent luminescence over photoluminescence for oilfield sensing applications.[16,20]

Upon exciting the $MgAl_{0.05}G_{0.95}O_3$:0.3%Pr^{3+} NPs dispersed in water at 254 nm for 5 min, persistent luminescence spectra were recorded, revealing a singular peak within the visible range, with a peak centered at 625 nm, as delineated in Figure 3b. Notably, the intensity of this peak exhibited a diminishing trend with decreasing NP concentration, as depicted in Figure S4.

Consequently, spectral acquisition at lower $MgAl_{0.05}G_{0.95}O_3$:0.3%Pr^{3+} NPs concentrations was found to be unfeasible due to the reduced sensitivity of the spectrofluorometer and the lower concentration of NPs. Therefore, an alternative approach utilizing a CCD camera-based imaging method was pursued,[20] as detailed in the following section.

3.2. Imaging Method. The challenges posed by the low sensitivity of the spectral method, coupled with the inherently low afterglow signals of $MgAl_{0.05}G_{0.95}O_3$:0.3%Pr^{3+} NPs in oil emulsions, compounded by the presence of a dense oil phase, hindered effective NPs excitation and subsequently led to lower detection of NPs within the emulsion. To address this, we turned to the IVIS Lumina III imaging system for enhanced detection of $MgAl_{0.05}G_{0.95}O_3$:0.3%Pr^{3+} NPs in the crude oil/water emulsion.[20,22]

Our experimental setup involved testing emulsions in quartz cuvettes, subjecting them to 254 nm UV light irradiation for 5 min. Subsequently, images were captured after 1 min of excitation using the bioluminescence mode, with various exposure times of 15 s, 30 s, and 1 min. The persistent luminescence images of the different concentrations (0, 1, 5, 10, 50, 100, and 1000 ppb) of $MgAl_{0.05}G_{0.95}O_3$:0.3%Pr^{3+} NPs within the 50/50 crude oil/water emulsions are shown in Figure 4a. As a control, the 50/50 crude oil/water emulsion without NPs was used to quantify the background noise from the oil/water emulsion. Remarkably, the imaging method enabled the visualization of NPs at concentrations as low as 1 ppb. Moreover, the brightness exhibited a proportional increase as the concentration of the NPs increased within the emulsion.[20,22]

Further analysis revealed a linear relationship between the average persistent luminescence intensity and the concentration of the $MgAl_{0.05}G_{0.95}O_3$:0.3%Pr^{3+} NPs, as depicted in Figure 4b. The average intensity was determined by processing the acquired images using the ROI tool in Living Image software, as outlined in Table S1.

https://doi.org/10.1021/acsomega.4c04281
ACS Omega 2024, 9, 38678−38685

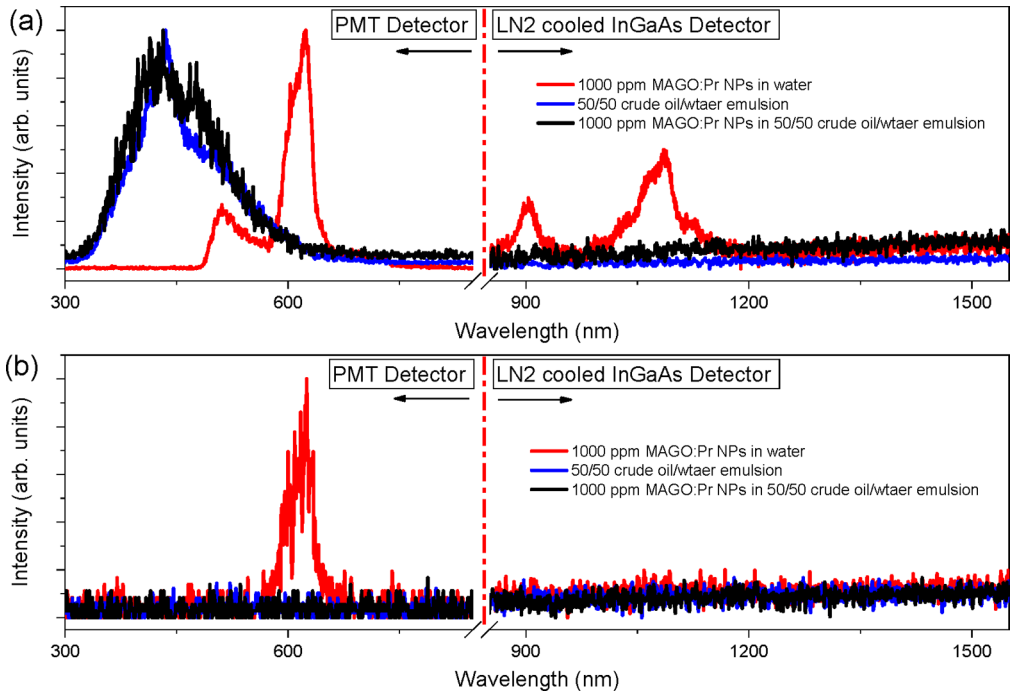

Figure 3. Spectral acquisition of $MgAl_{0.05}Ge_{0.95}O_3$:0.3%Pr^{3+} NPs, without and within crude oil/water emulsions. (a) Photoluminescence emission spectra of 1000 ppm of $MgAl_{0.05}Ge_{0.95}O_3$:0.3%Pr^{3+} NPs dispersed in DI water (red line), 50/50 crude oil/water emulsion (blue line), and 1000 ppm of $MgAl_{0.05}Ge_{0.95}O_3$:0.3%Pr^{3+} NPs in 50/50 crude oil/water emulsion (black line), under 260 nm excitation. (b) Persistent luminescence emission spectra of the 1000 ppm $MgAl_{0.05}Ge_{0.95}O_3$:0.3%Pr^{3+} NPs dispersed in DI water (red line), 50/50 crude oil/water emulsion (blue line), and 1000 ppm $MgAl_{0.05}Ge_{0.95}O_3$:0.3%Pr^{3+} NPs in 50/50 crude oil/water emulsion (black line), recorded after 1 min of ceasing the excitation at 254 nm UV radiation.

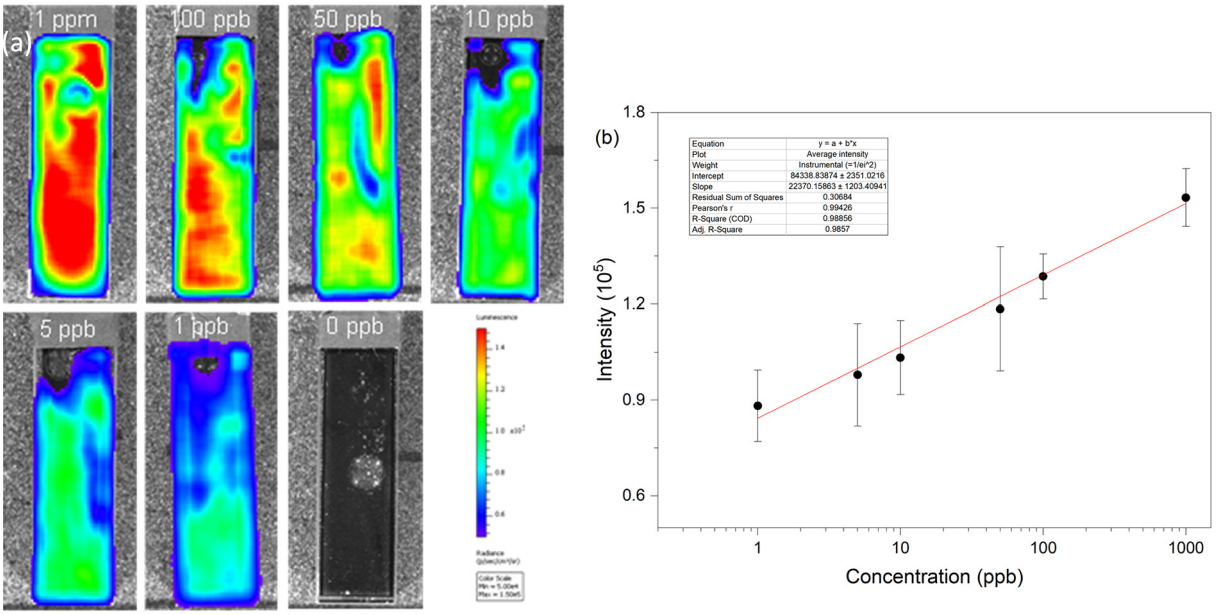

Figure 4. Detection of $MgAl_{0.05}G_{0.95}O$:0.3%Pr^{3+} NPs in a 50/50 crude oil/water emulsion. (a) Persistent luminescence images in the visible range of 1000, 100, 50, 10, 5, 1, 0.5, and 0 ppb $MgAl_{0.05}G_{0.95}O$:0.3%Pr^{3+} NPs in 50/50 (volume ratio) crude oil/water emulsions. The scale bar is in radiance, photon·second^{-1}·cm^{-2}·steradian^{-1}, (p/s/cm^2/sr). (b) Plot of the average persistent luminescence intensity of the $MgAl_{0.05}G_{0.95}O$:0.3% Pr^{3+} NPs in 50/50 crude oil/water emulsions as a function of $MgAl_{0.05}G_{0.95}O$:0.3%Pr^{3+} NPs concentration. The average intensity was calculated using the region of interest (ROI) tools.

4. CONCLUSIONS

In conclusion, $MgAl_{0.05}Ge_{0.95}O_3$:0.3%Pr^{3+} nanophosphors were successfully synthesized by the sol−gel method, offering an effective alternative to the traditional solid-state synthesis for such materials. The synthesized persistent phosphors exhibited luminescent emission across multiple regions of the electromagnetic spectrum, with peak emission at 625 nm in the visible region, 905 nm in the NIR region, and 1089 nm in the SWIR domain.

https://doi.org/10.1021/acsomega.4c04281
ACS Omega 2024, 9, 38678−38685

Detailed analysis of the persistent luminescence data revealed fascinating characteristics: upon excitation at 254 nm for 5 min, spectral readings could be obtained after 5 h, and the emission at 625 nm could be monitored after 15 h of the stoppage of the excitation. These findings underscore the intricate interplay among the dopant, host materials, and excitation mechanism, elucidating the nuanced photoluminescent behavior observed in $MgAl_{0.05}Ge_{0.95}O_3$:0.3%Pr^{3+} nanophosphor. Such insights highlight the material potential for diverse applications within optoelectronic devices.

Moreover, by employing spectral and imaging techniques, the prepared nanophosphors were successfully detected within the crude oil/water emulsion. Remarkably, the imaging method demonstrated sensitivity to concentrations as low as 1 ppb of the prepared material within the crude oil/water emulsion, showcasing its potential for precise detection and monitoring in complex environments. Through this research, the efficacy of these NPs in providing enduring luminescent signals has been demonstrated, paving the way for the improved monitoring and management of crude oil. Thus, the synthesis and application of persistent luminescent NPs have demonstrated their immense potential as sophisticated tools for tracing crude oil.

■ ASSOCIATED CONTENT

Supporting Information

The Supporting Information is available free of charge at https://pubs.acs.org/doi/10.1021/acsomega.4c04281.

XRD patterns of $MgGeO_3$:0.3%Pr^{3+} NPs, persistent luminescence decay curves at different wavelengths, persistent luminescence emission spectra, persistent luminescence emission spectra at different concentrations, and Table S1 with the average intensity at different concentrations of NPs (PDF)

■ AUTHOR INFORMATION

Corresponding Author

Syed Niaz Ali Shah − *Center for Integrative Petroleum Research, College of Petroleum Engineering and Geosciences, King Fahd University of Petroleum and Minerals, Dhahran 31261, Saudi Arabia;* orcid.org/0000-0001-9902-857X; Email: niazalianalyst@gmail.com, syed.shah.3@kfupm.edu.sa

Author

Yafei Chen − *Center for Integrative Petroleum Research, College of Petroleum Engineering and Geosciences, King Fahd University of Petroleum and Minerals, Dhahran 31261, Saudi Arabia*

Complete contact information is available at: https://pubs.acs.org/10.1021/acsomega.4c04281

Notes

The authors declare no competing financial interest.

■ ACKNOWLEDGMENTS

Y.C. acknowledges the financial support provided by the King Fahd University of Petroleum and Minerals (KFUPM) Startup Funding (SF23006).

■ REFERENCES

(1) Hölsä, J. Persistent luminescence beats the afterglow: 400 years of persistent luminescence. *Electrochemical Society Interface* **2009**, *18* (4), 42.

(2) Shionoya, S.; Yen, W. M.; Yamamoto, H. *Phosphor Handbook*; CRC Press, 2018.

(3) Van den Eeckhout, K.; Smet, P. F.; Poelman, D. Persistent Luminescence in Eu(2+)-Doped Compounds: A Review. *Materials (Basel)*. **2010**, *3* (4), 2536−2566.

(4) Matsuzawa, T.; Aoki, Y.; Takeuchi, N.; Murayama, Y. A new long phosphorescent phosphor with high brightness, $SrAl_2O_4$: Eu^{2+}, Dy^{3+}. *J. Electrochem. Soc.* **1996**, *143* (8), 2670.

(5) Lin, Y.; Tang, Z.; Zhang, Z.; Wang, X.; Zhang, J. Preparation of a new long afterglow blue-emitting $Sr_2MgSi_2O_7$-based photoluminescent phosphor. *Journal of materials science letters* **2001**, *20* (16), 1505−1506.

(6) Pan, Z.; Lu, Y.-Y.; Liu, F. Sunlight-activated long-persistent luminescence in the near-infrared from Cr^{3+}-doped zinc gallogermanates. *Nature materials* **2012**, *11* (1), 58−63.

(7) Liang, Y.; Liu, F.; Chen, Y.; Wang, X.; Sun, K.; Pan, Z. Extending the applications for lanthanide ions: efficient emitters in short-wave infrared persistent luminescence. *Journal of Materials Chemistry C* **2017**, *5* (26), 6488−6492.

(8) Liang, Y.-J.; Liu, F.; Chen, Y.-F.; Wang, X.-J.; Sun, K.-N.; Pan, Z. New function of the Yb3+ ion as an efficient emitter of persistent luminescence in the short-wave infrared. *Light: Science & Applications* **2016**, *5* (7), No. e16124.

(9) Zheng, S.; Shi, J.; Fu, X.; Wang, C.; Sun, X.; Chen, C.; Zhuang, Y.; Zou, X.; Li, Y.; Zhang, H. X-ray recharged long afterglow luminescent nanoparticles $MgGeO_3$: Mn^{2+}, Yb^{3+}, Li^+ in the first and second biological windows for long-term bioimaging. *Nanoscale* **2020**, *12* (26), 14037−14046.

(10) Shah, J.; Rasul Jan, M.; Shah, S.; Shah, Niaz Ali; S. Spectrofluorimetric determination of cephradine in commercial formulation using ethylacetoacetate-formaldehyde as fluorogenic agent. *J. Anal. Chem.* **2014**, *69* (7), 638−645.

(11) Shah, S. N. A.; Lin, J.-M. Recent advances in chemiluminescence based on carbonaceous dots. *Adv. Colloid Interface Sci.* **2017**, *241*, 24−36.

(12) Shah, S. N. A.; Gul, E.; Hayat, F.; Rehman, Z.; Khan, M. Advancement and Perspectives of Sulfite-Based Chemiluminescence, Its Mechanism, and Sensing. *Chemosensors* **2023**, *11* (4), 212.

(13) Srivastava, A. Aspects of Pr3+ luminescence in solids. *J. Lumin.* **2016**, *169*, 445−449.

(14) Itoh, S.; Toki, H.; Tamura, K.; Kataoka, F. A new red-emitting phosphor, $SrTiO_3$: Pr^{3+}, for low-voltage electron excitation. *Japanese journal of applied physics* **1999**, *38* (11R), 6387.

(15) Ferdous, A. R.; Shah, S. N. A.; Shah, S. S.; Aziz, M. A. Advancements in nanotechnology applications: Transforming catalysts, sensors, and coatings in petrochemical industries. *Fuel* **2024**, *371*, No. 132020.

(16) Murugesan, S.; Agrawal, D.; Suresh, R.; Khabashesku, V.; Darugar, Q. *Upconversion Nanoparticles as Tracers for Production and Well Monitoring*. In SPE Annual Technical Conference and Exhibition, 2018; D011S003R004, Vol. Day 1 Mon, September 24, 2018. .

(17) Kanj, M. Y.; Kosynkin, D. V. *Oil industry first field trial of interwell reservoir nanoagent tracers*. In Micro-and Nanotechnology Sensors, Systems, and Applications VII; International Society for Optics and Photonics, 2015; Vol. *9467*, p 94671D.

(18) Kanj, M. Y.; Rashid, M.; Giannelis, E. P. *Industry first field trial of reservoir nanoagents*. In SPE Middle East Oil and Gas Show and Conference, 2011; OnePetro.

(19) Wang, J.; Ma, Q.; Wang, Y.; Shen, H.; Yuan, Q. Recent progress in biomedical applications of persistent luminescence nanoparticles. *Nanoscale* **2017**, *9* (19), 6204−6218.

(20) Chuang, Y.-J.; Liu, F.; Wang, W.; Kanj, M. Y.; Poitzsch, M. E.; Pan, Z. Ultra-sensitive in-situ detection of near-infrared persistent luminescent tracer nanoagents in crude oil-water mixtures. *Sci. Rep.* **2016**, *6* (1), 27993.

(21) Murugesan, S.; Suresh, R.; Agrawal, D.; Darugar, Q.; Khabashesku, V. *Unconventional Nanotechnology-Based Tracers for Drilling and Completion Applications*. In International Petroleum Technology Conference, 2020; D021S025R002, Vol. Day 2 Tue, January 14, 2020. .
(22) Chen, Y.; Pan, Z. Red/NIR/SWIR multi-band persistent luminescent nanoparticles as ultrasensitive multi-channel tracers in water and crude oil/water emulsions. *Nano Research* **2023**, *16* (11), 12706−12712.
(23) Chuang, Y.-J.; Liu, F.; Wang, W.; Kanj, M. Y.; Poitzsch, M. E.; Pan, Z. Ultra-sensitive in-situ detection of near-infrared persistent luminescent tracer nanoagents in crude oil-water mixtures. *Sci. Rep.* **2016**, *6*, No. 27993.
(24) Li, Y.; Gecevicius, M.; Qiu, J. Long persistent phosphors—from fundamentals to applications. *Chem. Soc. Rev.* **2016**, *45* (8), 2090−2136.
(25) Liang, Y.; Liu, F.; Chen, Y.; Wang, X.; Sun, K.; Pan, Z. Red/near-infrared/short-wave infrared multi-band persistent luminescence in Pr^{3+}-doped persistent phosphors. *Dalton Transactions* **2017**, *46* (34), 11149−11153.
(26) Leinenweber, K.; Wang, Y.; Yagi, T.; Yusa, H. An unquenchable perovskite phase of $MgGeO_3$ and comparison with $MgSiO_3$ perovskite. *Am. Mineral.* **1994**, *79* (1−2), 197−199.
(27) Ross, N. L.; Navrotsky, A. Study of the MgGeO 3 polymorphs (orthopyroxene, clinopyroxene, and ilmenite structures) by calorimetry, spectroscopy, and phase equilibria. *Am. Mineral.* **1988**, *73* (11−12), 1355−1365.
(28) Singh, M. Luminescent materials for communication devices: an overview. *Int. J. Eng. Technol. Manage. Res.* **2018**, *5* (2), 96−100. (acccessed 2024/06/17)
(29) Van den Eeckhout, K.; Smet, P. F.; Poelman, D. Persistent luminescence in Eu2+-doped compounds: a review. *Materials* **2010**, *3* (4), 2536−2566.
(30) Srivastava, A. M.; Renero-Lecuna, C.; Santamaría-Pérez, D.; Rodríguez, F.; Valiente, R. Pressure-induced Pr3+ 3P0 luminescence in cubic Y2O3. *Journal of luminescence* **2014**, *146*, 27−32.
(31) Huang, X.; Zhao, X.; Yu, Z.; Liu, Y.; Wang, A.; Wang, X.-j.; Liu, F. Effect of electron-transfer quenching on the photoluminescence of Pr 3+ in MgXO 3 (X= Ge, Si). *Optical Materials Express* **2020**, *10* (5), 1163−1168.
(32) Dorenbos, P.; Krumpel, A.; Van der Kolk, E.; Boutinaud, P.; Bettinelli, M.; Cavalli, E. Lanthanide level location in transition metal complex compounds. *Opt. Mater.* **2010**, *32* (12), 1681−1685.
(33) Boutinaud, P.; Pinel, E.; Oubaha, M.; Mahiou, R.; Cavalli, E.; Bettinelli, M. Making red emitting phosphors with Pr^{3+}. *Opt. Mater.* **2006**, *28* (1−2), 9−13.
(34) Kong, L.; Liu, Y.; Dong, L.; Zhang, L.; Qiao, L.; Wang, W.; You, H. Near-infrared emission of $CaAl_6Ga_6O_{19}$:Cr^{3+},Ln^{3+} (Ln = Yb, Nd, and Er) via energy transfer for c-Si solar cells. *Dalton Transactions* **2020**, *49* (25), 8791−8798.
(35) Alam, P.; Leung, N. L. C.; Liu, J.; Cheung, T. S.; Zhang, X.; He, Z.; Kwok, R. T. K.; Lam, J. W. Y.; Sung, H. H. Y.; Williams, I. D.; et al. Two Are Better Than One: A Design Principle for Ultralong-Persistent Luminescence of Pure Organics. *Adv. Mater.* **2020**, *32* (22), No. 2001026.
(36) Paterson, A. S.; Raja, B.; Garvey, G.; Kolhatkar, A.; Hagström, A. E. V.; Kourentzi, K.; Lee, T. R.; Willson, R. C. Persistent Luminescence Strontium Aluminate Nanoparticles as Reporters in Lateral Flow Assays. *Anal. Chem.* **2014**, *86* (19), 9481−9488.

https://doi.org/10.1021/acsomega.4c04281
ACS Omega 2024, 9, 38678−38685